Fully Decentralized Controller for Multi-Robot Collective Transport in Space Applications

Hamed Farivarnejad
Arizona State University
Tempe, USA
hamed.farivarnejad@asu.edu

Amir Salimi Lafmejani
Arizona State University
Tempe, USA
asalimil@asu.edu

Spring Berman
Arizona State University
Tempe, USA
spring.berman@asu.edu

Abstract*—In this paper, we propose a fully decentralized control strategy for collective payload transport in 3D space by a team of identical holonomic mobile robots in a microgravity environment. This task has potential space applications such as on-orbit assembly, debris removal, and planetary construction, which have to be performed in uncertain environments where inter-robot communication is unreliable or not available. Decentralized control schemes that rely on limited data and do not require inter-robot communication would enable teams of robots to achieve cooperative transport objectives in unknown environments. Existing decentralized strategies for collective payload transport require at least some of the following information: (1) the geometry and dynamics of the payload; (2) the payload's position and velocity over time; (3) the number and distribution of robots around the payload; (4) the vector from the payload's center of mass to each robot's attachment point; and (5) desired trajectories for the robots and payload. In this paper, we consider a team of robots that must stabilize a payload's center of mass to a target position without access to any of this information. The robots are assumed to be rigidly attached to the payload, e.g. via pincers, grippers, or magnets, and the only information provided to them is the target position in a global coordinate system that is shared by all the robots. The robots do not exchange information and only require measurements of their own positions and velocities. Moreover, the payload may have an arbitrary shape, without particular constraints on its geometry (e.g., convexity). Given these assumptions and objectives, and building on our prior work on collective transport strategies, we design a fully decentralized proportional-derivative controller that can be employed by the robots to drive the payload's center of mass to the destination. Using a Lyapunov stability argument, we analytically prove that under this controller, the payload's center of mass asymptotically converges to a small neighborhood of the target position. The radius of this neighborhood is the magnitude of the error between the target position and actual steady-state position of the payload's center of mass. We also investigate the effect of the distribution of robots around the payload on the magnitude of this error. We validate our theoretical results in MATLAB simulations of five collective transport scenarios with different payload shapes and variations in the distribution of robots around the payload.

TABLE OF CONTENTS

This work was supported by the Arizona State University Global Security Initiative.

H. Farivarnejad and S. Berman are with School for Engineering of Matter, Transport and Energy, Arizona State University (ASU), Tempe, AZ 85287, email: {hamed.farivarnejad, spring.berman}@asu.edu. A. Salimi Lafmejani is with the School of Electrical, Computer and Energy Engineering, ASU, Tempe, AZ, 85287, email: asalimil@asu.edu.

2021 IEEE Aerospace Conference | 978-1-7281-7436-5/21/$31.00 ©2021 IEEE | DOI: 10.1109/AERO50100.2021.9438133

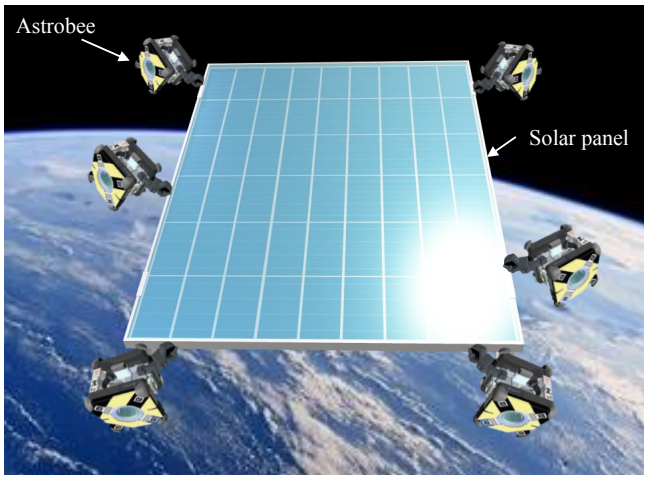

Figure 1: Conceptual illustration of on-orbit collective transport of a 3D payload (solar panel) by six Astrobee robots.

1. INTRODUCTION

Multiple robots can be used to accomplish complicated tasks that cannot be accomplished by an individual robot [1]. Due to this capability, a system of multiple robots can be used in various applications such as construction, assembly, search-and-rescue operations, disaster response, and object transportation. Recently, various robotic systems have been used frequently in different space applications, including planetary exploration and on-orbit servicing [2], [3], [4], [5], [6].

On-orbit servicing tasks [7], [8], [9] such as moving irregular-shaped objects and assembly of large heavy space structures [10] require cooperative object manipulation, also called *collective transport*, by multiple robots. Figure 1 shows a conceptual illustration of an on-orbit collective transport task in which six Astrobee [11] robots cooperatively manipulate a solar panel in space (Astrobee image is from [5]). Collective transport approaches that rely on inter-robot communication are vulnerable to failures arising from communication delays, bandwidth limitations, and loss of connectivity. Moreover, in order to implement a versatile, cost-effective multi-robot system that can handle many types of payloads with minimal sensing capabilities, the control strategy should not require the robots to have information about their distribution around the payload or the payload's mass, geometry, or motion. Centralized or distributed control approaches which rely on inter-robot communication and knowledge about the payload dynamics cannot be applied in these scenarios. Instead, it will be necessary to use a fully decentralized control approach in which each robot employs a controller that only requires local sensing information and there is no communication between the robots.

In this paper, we propose a fully decentralized control approach that is inspired by the phenomenon of group food retrieval in ants [12], [13], [14]. This behavior is an example of decentralized cooperative manipulation in which the transporters do *not* use explicit communication, follow predefined trajectories to the goal point, or have prior knowledge about the payload's properties and the number and distribution of transporters around the payload [15]. In our control approach, the individual actions of the robots during collective transport are determined by their locally perceived information as they navigate to the goal point. We design decentralized position controllers for a collective transport task in 3D space by a group of point-mass robots that lack inter-robot communication and can only use on-board measurements of their own positions and velocities as feedback. The controllers have a proportional-derivative (PD) structure and drive the robots to transport the payload to a target destination.

Related Work

Multi-robot systems for space applications have been investigated in many research studies. For instance, a control approach for multiple satellites to perform area coverage and space exploration is presented in [16]. As another example, reconfigurable modular robots are conceptualized for on-orbit satellite servicing in [17]. In [18], a human-supervised team of robots is proposed for assembly of structures in orbit or on planetary surfaces. In [19], a control approach is presented for manipulation of objects in 3D by orbital free-flying robots.

There are numerous studies on designing control approaches for cooperative transport tasks by multiple mobile manipulators in aerial, terrestrial, and underwater environments. Decentralized control approaches for collective transport have previously been proposed for scenarios in which the robots follow preplanned trajectories or have information about the geometry and dynamics of the payload, the payload's position and velocity or the distribution and number of robots carrying the payload. In the decentralized approach proposed in [20], robots push a large payload to a goal when their line of sight to the goal is occluded by the payload. The strategies described in [21], [22], require robots to communicate their measurements to one another in order to estimate the dynamics of the payload. In [23], the authors propose an event-triggered communication strategy with distributed impedance control to improve the stability and robustness of cooperative manipulation of unknown payloads in unknown environments.

Adaptive robust control approaches have been proposed for cooperative manipulation in 2D and 3D. These approaches combine a stabilizing term with a regression term in the controller in order to achieve stabilization in the presence of parameter uncertainties. However, these approaches require either prior information about the robots' distribution around the payload or feedback on the payload's motion [24], [25], [26]. In [27], an approach is presented for pose control of a rod-shaped object using cooperative aerial manipulation, in which the robot trajectories are preplanned. A similar control approach for cooperative aerial manipulation in [28] requires a global positioning system and real-time planning. In [29], a networked control method with decoupled robot dynamics is presented for collective transport by mobile manipulators with communication. In [30], decentralized collaborative manipulation of rigid bodies in both 2D and 3D is achieved using an adaptive control approach that requires predefined payload trajectories and knowledge of the position and velocity of the payload's center of mass. A decentralized approach for cooperative manipulation is proposed in [31] in which the robots have a common reference model for the desired payload motion and use an adaptive controller to compensate for the effect of friction on the payload. This approach requires the robots to have access to measurements of the payload's linear and angular velocities, whereas our approach does not require any information on the payload's motion.

Control approaches for collective transport that do not require inter-robot communication or prior knowledge about the payload dynamics have also been developed [32], [33], but they rely on predefined robot and payload trajectories that are planned by a global supervisor. In [34], a strategy inspired by a leader-follower scheme is presented for transport of a flexible payload that is based on implicit communication and requires knowledge of the payload dynamics. A strategy for cooperative aerial manipulation and transport of large and heavy objects is proposed in [35], which requires the robots to estimate dynamic parameters of the payload. Recently, learning-based methods have also been proposed for collective transport tasks. In [36], robots in a transport team, which explicitly exchange information, jointly reach the same desired motion by running a time-varying quadratic program which is solved online by a neural network scheme. A dynamic recurrent neural network is used in [37] to solve a quadratic program that computes cooperative kinematic controllers for redundant manipulators using partially known information about the payload and the teammates. In addition, reinforcement learning is used in [38] to design two distributed approaches to cooperative manipulation: the first applies Q-learning with individual reward functions, and the second utilizes game-theoretic techniques. The first approach exhibits more robustness to different reward structures than the second.

In our prior work [39], we addressed the problem of controlling the velocity of a payload, rather than its position, for a multi-robot transport team without knowledge about the payload or inter-robot communication. Moreover, in our most recent work [40], we proposed a proportional-derivative (PD) controller for collective transport in 2D that does not rely on inter-robot communication, prior knowledge about the load dynamics and geometry, or knowledge of the number of robots and their distribution around the payload. We proved that under this control strategy, the payload's rotation is bounded and its angular velocity converges to zero. In this paper, we extend our previous work to collective transport tasks in 3D that are useful for on-orbit servicing and space applications. We analytically prove asymptotic convergence of the payload's center of mass to a neighborhood of the target position and study the parameters that influence the steady-state distance between the payload's center of mass and this goal position.

Paper Organization

The organization of the paper is as follows. In Section 2, we describe the problem statement and derive the dynamical model of the multi-robot transport system. In Section 3, we present our fully decentralized control approach and analyze the stability and convergence properties of the closed-loop system dynamics. In Section 4, we validate our control approach in simulations of five different scenarios in which a team of Astrobee robots cooperatively transport a 3D object to a target location.

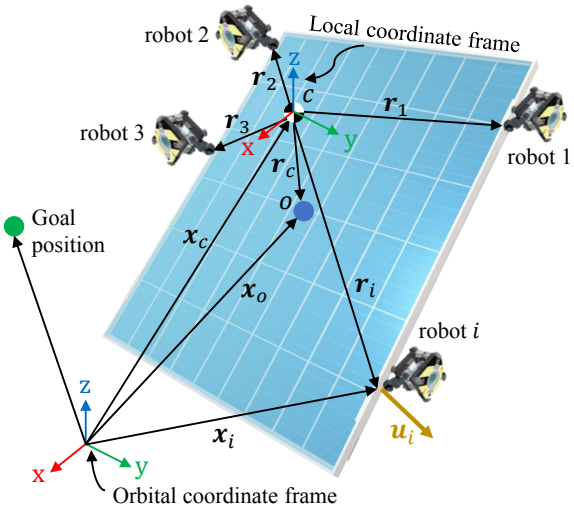

Figure 2: Illustration of an orbital coordinate frame and a local coordinate frame fixed to the payload, as well as geometric parameters that express the position of a robot in the payload's local coordinate frame.

2. PRELIMINARIES

In this section, we first present the collective transport problem statement and associated notation. Then, we derive the equations that describe the orbital dynamics of the entire system, consisting of the robots and the payload.

Problem Statement

We consider a team of N identical point-mass robots that move in 3D space and are rigidly attached to a payload in an arbitrary configuration, as shown in Fig. 2. We assume that each robot has access to its own position and velocity with respect to an orbital coordinate system, which is common to all the robots.[2] The robots do not communicate with one another and are not assigned predefined trajectories. They also lack information about the payload's kinematics and dynamics, the number of robots in the transport team, and the robots' distribution around the payload.

We define $\boldsymbol{x}_o = [x_o\ y_o\ z_o]^T \in \mathbb{R}^3$ and $\boldsymbol{\delta}_o = [\phi_o\ \theta_o\ \psi_o]^T \in \mathbb{R}^3$ as the position of the payload's center of mass, point O in Fig. 2, and the payload's orientation with respect to the orbital coordinate frame, respectively. We define $\boldsymbol{x}_i = [x_i\ y_i\ z_i]^T \in \mathbb{R}^3$ as the position of robot i and $\boldsymbol{x}_d = [x_d\ y_d\ z_d]^T \in \mathbb{R}^3$ as the position of the target point in the orbital frame, as shown in Fig. 2. The center of mass of the entire system, including both the load and the robots, is denoted by point C in Fig. 2. Given that points O and C are not necessarily coincident, we define $\boldsymbol{x}_c = [x_c\ y_c\ z_c]^T \in \mathbb{R}^3$ as the position of C in the orbital frame and $\boldsymbol{r}_c \in \mathbb{R}^3$ as the vector from C to O, as shown in Fig. 2. We also define $\boldsymbol{r}_i = [r_{ix}\ r_{iy}\ r_{iz}]^T \in \mathbb{R}^3$ as the vector from C to the attachment point of robot i in the payload's local coordinate frame.

Each robot i knows its own position $\boldsymbol{x}_i$ and velocity $\dot{\boldsymbol{x}}_i$ and applies an actuating force $\boldsymbol{u}_i = [u_{ix}\ u_{iy}\ u_{iz}]^T \in \mathbb{R}^3$ to the payload, which we represent in the orbital frame. The control objective is to design the forces $\boldsymbol{u}_i$, $i = 1, ..., N$, such that the robots drive the position of the payload's center of mass, $\boldsymbol{x}_o$, to the target position $\boldsymbol{x}_d$. The only sensor feedback available to the robots consists of their on-board measurements of their own positions and velocities with respect to the orbital frame.

[2] An orbital coordinate system that is associated with a particular orbit moves at a velocity with respect to Earth at which objects in that orbit experience the microgravity condition. In this case, we can assume that the orbital coordinate system is fixed to the main spacecraft that deploys the robots for the collective transport task.

Dynamical Model

To derive the equations describing the orbital dynamics of the entire system, comprised of both the load and the robots, we use the framework in our previous papers [41], [39]. We consider a local coordinate frame whose origin is located at the center of mass of the entire system (C in Fig. 2). The axes of the local frame are chosen to be along the principal axes of the entire system. We denote the mass of each robot and the mass of the payload by m_r and m_o, respectively. We also define $\boldsymbol{J} \in \mathbb{R}^{3\times3}$ as the matrix of the moment of inertia of the entire system in the local coordinate frame. To this end, m and $\boldsymbol{J}$ are given by

$$\begin{aligned} m =& m_o + N m_r, \\ \boldsymbol{J} =& \boldsymbol{J}_o + m_o \left((\boldsymbol{r}_c^T \boldsymbol{r}_c)\boldsymbol{I} - \boldsymbol{r}_c \times \boldsymbol{r}_c \right) \\ &+ m_r \sum_{i=1}^{N} \left((\boldsymbol{r}_i^T \boldsymbol{r}_i)\boldsymbol{I} - \boldsymbol{r}_i \times \boldsymbol{r}_i \right), \end{aligned} \tag{1}$$

where $\boldsymbol{J}_o \in \mathbb{R}^{3\times3}$ is the payload's moment of inertia in the local coordinate system, and $\boldsymbol{I} \in \mathbb{R}^{3\times3}$ is the identity matrix. We define ${}^G\boldsymbol{R}_B \in \mathbb{R}^{3\times3}$ as the rotation matrix from the local frame to the orbital coordinate frame, which is a function of the payload's orientation, *i.e.* ${}^G\boldsymbol{R}_B = {}^G\boldsymbol{R}_B(\boldsymbol{\delta}_o)$. We also denote the angular velocity of the payload in the local frame by $\boldsymbol{\omega}_o \in \mathbb{R}^3$. Considering the entire system as a rigid body, we can write the equation of motion of the entire system as

$$\boldsymbol{M}\ddot{\boldsymbol{x}}_c = \sum_{i=1}^{N} \boldsymbol{u}_i \tag{2}$$

$$\boldsymbol{J}\dot{\boldsymbol{\omega}}_o + \hat{\boldsymbol{\omega}}_o \boldsymbol{J}\boldsymbol{\omega}_o = \sum_{i=1}^{N} \hat{\boldsymbol{r}}_i^G \boldsymbol{R}_B^T \boldsymbol{u}_i, \tag{3}$$

where $\hat{\boldsymbol{\omega}}_o \in SO(3)$ and $\hat{\boldsymbol{r}}_i \in SO(3)$ are the skew-symmetric representations of $\boldsymbol{\omega}_o$ and $\boldsymbol{r}_i$, respectively. We note that the weight of the payload and the robots are not incorporated into the dynamical model since we assume that the task is performed in a microgravity environment.

3. CONTROLLER DESIGN AND ANALYSIS

In this section, we present decentralized robot controllers for the system described by Eq. (2) and Eq. (3) that produce asymptotic convergence of the payload's center of mass to a neighborhood of the desired position $\boldsymbol{x}_d$.

Decentralized Control Law

The proposed control law has a proportional-derivative (PD) structure,

$$\boldsymbol{u}_i = -\boldsymbol{K}_d \dot{\boldsymbol{x}}_i - \boldsymbol{K}_p(\boldsymbol{x}_i - \boldsymbol{x}_d), \tag{4}$$

in which $\boldsymbol{K}_p = K_p\boldsymbol{I}$ and $\boldsymbol{K}_d = K_d\boldsymbol{I}$ are gain matrices, where $\boldsymbol{I} \in \mathbb{R}^{3\times3}$ is the identity matrix, and K_p and K_d are strictly positive constants. This control law implies that each robot *selfishly* tries to stabilize its own position to the target

position. Since the robots are attached to distinct points on the payload's boundary, convergence of all the robots' positions to the target position is impossible. However, by each applying the decentralized controller in Eq. (4), the robots produce a collective transport behavior that approximately achieves the control objective defined in Section 2. We analyze and discuss this behavior in the next section.

To analyze the collective behavior of the entire system of the payload and robots with the proposed controller, we first derive the dynamics of the closed-loop system and then investigate the stability and convergence properties of this system.

Closed-Loop Dynamics

There is a holonomic kinematic constraint between the position of robot i and the position of the system's center of mass (see Fig. 2), given by

$$\boldsymbol{x}_i = \boldsymbol{x}_c +^G \boldsymbol{R}_B \boldsymbol{r}_i. \tag{5}$$

Taking the time derivative of Eq. (5), we obtain

$$\dot{\boldsymbol{x}}_i = \dot{\boldsymbol{x}}_c +^G \boldsymbol{R}_B \hat{\boldsymbol{\omega}}_o \boldsymbol{r}_i, \tag{6}$$

where ${}^G\boldsymbol{R}_B\hat{\boldsymbol{\omega}}_o$ is the time derivative of ${}^G\boldsymbol{R}_B$ (see [42]) and represents the effect of the payload's rotation on the robots' velocities. We define $\boldsymbol{e}_c := \boldsymbol{x}_c - \boldsymbol{x}_d$, where $\dot{\boldsymbol{e}}_c = \dot{\boldsymbol{x}}_c$ and $\ddot{\boldsymbol{e}}_c = \ddot{\boldsymbol{x}}_c$, since $\boldsymbol{x}_d$ is constant. Substituting the expressions for $\boldsymbol{x}_i$ and $\dot{\boldsymbol{x}}_i$ in Eqs. 5 and 6 into Eq. (4), we obtain

$$\boldsymbol{u}_i = -\boldsymbol{K}_d(\dot{\boldsymbol{e}}_c +^G \boldsymbol{R}_B \hat{\boldsymbol{\omega}}_o \boldsymbol{r}_i) - \boldsymbol{K}_p(\boldsymbol{e}_c +^G \boldsymbol{R}_B \boldsymbol{r}_i). \tag{7}$$

We now incorporate the decentralized control law for $\boldsymbol{u}_i$ in Eq. (7) into the dynamical model in Eq. (2) and Eq. (3) to derive the equation of motion of the closed-loop system as

$$\begin{aligned} \boldsymbol{M}\ddot{\boldsymbol{e}}_c =& -\boldsymbol{K}_d \sum_{i=1}^{N} (\dot{\boldsymbol{e}}_c +^G \boldsymbol{R}_B \hat{\boldsymbol{\omega}}_o \boldsymbol{r}_i) \\ & - \boldsymbol{K}_p \sum_{i=1}^{N} (\boldsymbol{e}_c +^G \boldsymbol{R}_B \boldsymbol{r}_i), \end{aligned} \tag{8}$$

$$\begin{aligned} \boldsymbol{J}\dot{\boldsymbol{\omega}}_o =& -\sum_{i=1}^{N} \hat{\boldsymbol{r}}_i^G \boldsymbol{R}_B^T \boldsymbol{K}_d (\dot{\boldsymbol{e}}_c +^G \boldsymbol{R}_B \hat{\boldsymbol{\omega}}_o \boldsymbol{r}_i) \\ & - \sum_{i=1}^{N} \hat{\boldsymbol{r}}_i^G \boldsymbol{R}_B^T \boldsymbol{K}_p (\boldsymbol{e}_c +^G \boldsymbol{R}_B \boldsymbol{r}_i) \\ & - \hat{\boldsymbol{\omega}}_o \boldsymbol{J} \boldsymbol{\omega}_o, \end{aligned} \tag{9}$$

where $\boldsymbol{M} = m\boldsymbol{I}$. Taking into account the facts that ${}^G\boldsymbol{R}_B^T\,{}^G\boldsymbol{R}_B = \boldsymbol{I}$, $\hat{\boldsymbol{r}}_i \boldsymbol{r}_i = \boldsymbol{0}$, and $\hat{\boldsymbol{\omega}}_o \boldsymbol{r}_i = -\hat{\boldsymbol{r}}_i \boldsymbol{\omega}_o$, the closed-loop system in Eq. (8) and Eq. (9) can be rewritten as

$$\begin{aligned} \boldsymbol{M}\ddot{\boldsymbol{e}}_c =& -N(\boldsymbol{K}_d \dot{\boldsymbol{e}}_c + \boldsymbol{K}_p \boldsymbol{e}_c) - \boldsymbol{K}_d^G \boldsymbol{R}_B \hat{\boldsymbol{\omega}}_o \boldsymbol{\varrho} \\ & - \boldsymbol{K}_p^G \boldsymbol{R}_B \boldsymbol{\varrho}, \end{aligned} \tag{10}$$

$$\begin{aligned} \boldsymbol{J}\dot{\boldsymbol{\omega}}_o =& -\hat{\boldsymbol{\varrho}}^G \boldsymbol{R}_B^T (\boldsymbol{K}_d \dot{\boldsymbol{e}}_c + \boldsymbol{K}_p \boldsymbol{e}_c) - \boldsymbol{K}_d \boldsymbol{D} \boldsymbol{\omega}_o \\ & - \hat{\boldsymbol{\omega}}_o \boldsymbol{J} \boldsymbol{\omega}_o, \end{aligned} \tag{11}$$

where $\boldsymbol{\varrho} \in \mathbb{R}^3$, $\hat{\boldsymbol{\varrho}} \in SO(3)$, and $\boldsymbol{D} \in \mathbb{R}^{3\times 3}$ are given by

$$\boldsymbol{\varrho} := \sum_{i=1}^{N} \boldsymbol{r}_i \ , \quad \hat{\boldsymbol{\varrho}} := \sum_{i=1}^{N} \hat{\boldsymbol{r}}_i \ , \quad \boldsymbol{D} := \sum_{i=1}^{N} \hat{\boldsymbol{r}}_i^T \hat{\boldsymbol{r}}_i. \tag{12}$$

We can confirm that the vector and the matrices in Eq. (12) are constant since $\boldsymbol{r}_i$ is a constant vector in the payload's local coordinate system. Also, $\boldsymbol{D}$ is a positive definite matrix.

Convergence Analysis

The equilibrium state of the closed-loop system in Eq. (8) and Eq. (9) is obtained by setting $\ddot{\boldsymbol{e}}_c = \dot{\boldsymbol{e}}_c = \boldsymbol{0}$ and $\dot{\omega} = \omega = \boldsymbol{0}$, which results in the following equations:

$$N\boldsymbol{e}_c^* +^G \boldsymbol{R}_B^* \boldsymbol{\varrho} = \boldsymbol{0}, \tag{13}$$

$$\hat{\boldsymbol{\varrho}}^B \boldsymbol{R}_G^* \boldsymbol{K}_p \boldsymbol{e}_c^* = 0, \tag{14}$$

in which the superscript * denotes the equilibrium state. Solving Eq. (13) for $\boldsymbol{e}_c^*$, we obtain $\boldsymbol{e}_c^* = -\frac{1}{N}{}^G\boldsymbol{R}_B^* \boldsymbol{\varrho}$. We can confirm that $\hat{\boldsymbol{\varrho}}\boldsymbol{\varrho} = \boldsymbol{0}$. This shows that Eq. (14) is redundant. Also, since $\boldsymbol{\varrho}$ is constant, and a rotation matrix never changes the norm of a vector that it multiplies, the steady-state error $\boldsymbol{e}_c^*$ has a constant magnitude. The set of equilibrium states $\mathcal{E}$ is therefore obtained as

$$\mathcal{E} = \left\{ \boldsymbol{e}_{\mathrm{c}}, \dot{\boldsymbol{e}}_{\mathrm{c}}, \boldsymbol{\delta}_{\mathrm{o}}, \boldsymbol{\omega}_{\mathrm{o}} \in \mathbb{R}^3 \mid \boldsymbol{e}_{\mathrm{c}} = -\frac{1}{N}{}^{\mathrm{G}}\boldsymbol{R}_{\mathrm{B}}^* \boldsymbol{\varrho},\ \dot{\boldsymbol{e}}_{\mathrm{c}} = \boldsymbol{\omega}_{\mathrm{o}} = \boldsymbol{0} \right\}. \tag{15}$$

Note that the payload's orientation $\boldsymbol{\delta}_o$ is not specified in $\mathcal{E}$, which means that $\mathcal{E}$ is a manifold in the state space and not an isolated equilibrium point. To analyze the convergence of the closed-loop system's trajectories to $\mathcal{E}$, we consider the following quadratic positive semidefinite function,

$$\begin{aligned} V =& \frac{1}{2N}(N\boldsymbol{e}_c +^G \boldsymbol{R}_B \boldsymbol{\varrho})^T \boldsymbol{K}_p (N\boldsymbol{e}_c +^G \boldsymbol{R}_B \boldsymbol{\varrho}) \\ & + \frac{1}{2}\dot{\boldsymbol{e}}_c^T \boldsymbol{M} \dot{\boldsymbol{e}}_c + \frac{1}{2}\boldsymbol{\omega}_o^T \boldsymbol{J} \boldsymbol{\omega}_o, \end{aligned} \tag{16}$$

which is zero in the set $\mathcal{E}$ and positive everywhere else. The time derivative of V is calculated as

$$\begin{aligned} \dot{V} =& \frac{1}{N}(N\boldsymbol{e}_c +^G \boldsymbol{R}_B \boldsymbol{\varrho})^T \boldsymbol{K}_p (N\dot{\boldsymbol{e}}_c +^G \boldsymbol{R}_B \dot{\boldsymbol{\varrho}} +^G \dot{\boldsymbol{R}}_B \boldsymbol{\varrho}) \\ & + \dot{\boldsymbol{e}}_c^T \boldsymbol{M} \ddot{\boldsymbol{e}}_c + \boldsymbol{\omega}_o^T \boldsymbol{J} \dot{\boldsymbol{\omega}}_o \ . \end{aligned} \tag{17}$$

Taking into account the facts that ${}^G\dot{\boldsymbol{R}}_B = {}^G\boldsymbol{R}_B \hat{\boldsymbol{\omega}}_o$ and $\dot{\boldsymbol{\varrho}} = \boldsymbol{0}$, Eq. (17) can be written as

$$\begin{aligned} \dot{V} =& \dot{\boldsymbol{e}}_c^T \left(-N(\boldsymbol{K}_d \dot{\boldsymbol{e}}_c + \boldsymbol{K}_p \boldsymbol{e}_c) - \boldsymbol{K}_d^G \boldsymbol{R}_B \hat{\boldsymbol{\omega}}_o \boldsymbol{\varrho} - \boldsymbol{K}_p^G \boldsymbol{R}_B \boldsymbol{\varrho} \right) \\ & - \boldsymbol{\omega}_o^T \left(\hat{\boldsymbol{\varrho}}^G \boldsymbol{R}_B^T (\boldsymbol{K}_d \dot{\boldsymbol{e}}_c + \boldsymbol{K}_p \boldsymbol{e}_c) + \boldsymbol{K}_d \boldsymbol{D} \boldsymbol{\omega}_o + \hat{\boldsymbol{\omega}}_o \boldsymbol{J} \boldsymbol{\omega}_o \right) \\ & + N\boldsymbol{e}_c^T \boldsymbol{K}_p \dot{\boldsymbol{e}}_c + \boldsymbol{e}_c^T \boldsymbol{K}_p^G \boldsymbol{R}_B \hat{\boldsymbol{\omega}}_o \boldsymbol{\varrho} + \boldsymbol{\varrho}^T {}^G\boldsymbol{R}_B^T \boldsymbol{K}_p \dot{\boldsymbol{e}}_c \\ & + \frac{1}{N}\boldsymbol{\varrho}^T {}^G\boldsymbol{R}_B^T \boldsymbol{K}_p^G \boldsymbol{R}_B \hat{\boldsymbol{\omega}}_o \boldsymbol{\varrho}. \end{aligned} \tag{18}$$

We see that many terms in the above expression cancel out. Moreover, since $\hat{\boldsymbol{\omega}}_o$ is skew-symmetric and $\boldsymbol{J}$ is diagonal, the term $\boldsymbol{\omega}_o^T \hat{\boldsymbol{\omega}}_o \boldsymbol{J} \boldsymbol{\omega}_o$ and the last term in the right-hand side of Eq. (18) are zero. Hence, $\dot{V}$ is simplified to

$$\begin{aligned} \dot{V} =& -N\dot{\boldsymbol{e}}_c^T \boldsymbol{K}_d \dot{\boldsymbol{e}}_c - \dot{\boldsymbol{e}}_c^T \boldsymbol{K}_d^G \boldsymbol{R}_B \hat{\boldsymbol{\omega}}_o \boldsymbol{\varrho} - \boldsymbol{\omega}_o^T \hat{\boldsymbol{\varrho}}^G \boldsymbol{R}_B^T \boldsymbol{K}_d \dot{\boldsymbol{e}}_c \\ & - \boldsymbol{\omega}_o^T \boldsymbol{K}_d \boldsymbol{D} \boldsymbol{\omega}_o. \end{aligned} \tag{19}$$

Using the facts that $\hat{\boldsymbol{\varrho}}^T = -\hat{\boldsymbol{\varrho}}$ and $\hat{\boldsymbol{\omega}}_o\boldsymbol{\varrho} = -\hat{\boldsymbol{\varrho}}\boldsymbol{\omega}_o$, Eq. (19) can be rewritten in the following quadratic form:

$$\dot{V} = -\begin{bmatrix}\dot{\boldsymbol{e}}_c^T & \boldsymbol{\omega}_o^T\end{bmatrix} \underbrace{\begin{bmatrix} N\boldsymbol{K}_d & -\boldsymbol{K}_d^G\boldsymbol{R}_B\hat{\boldsymbol{\varrho}} \\ \hat{\boldsymbol{\varrho}}^G\boldsymbol{R}_B^T\boldsymbol{K}_d & \boldsymbol{K}_d\boldsymbol{D}\end{bmatrix}}_{\boldsymbol{Q}} \begin{bmatrix}\dot{\boldsymbol{e}}_c \\ \boldsymbol{\omega}_o\end{bmatrix}. \quad (20)$$

We can confirm that the matrix $\boldsymbol{Q} \in \mathbb{R}^{6\times6}$ is symmetric positive definite. This shows that $\dot{V}$ is negative semi-definite, and henceforth V remains bounded throughout the motion of the entire system. Furthermore, invoking *LaSalle's invariance principle* [43], we can conclude that the trajectories of the closed-loop system in Eq. (10) and Eq. (11) converge to a set that is characterized by $\dot{V} \equiv 0$, for which $\dot{\boldsymbol{e}}_c \equiv \boldsymbol{0}$ and $\boldsymbol{\omega}_o \equiv 0$. This is the set $\mathcal{E}$ in Eq. (15). Convergence of the closed-loop system's trajectories to $\mathcal{E}$ implies that as $t \to \infty$, the center of mass of the entire system (C) converges to a neighborhood of the target position $\boldsymbol{x}_d$ and the payload's angular velocity $\boldsymbol{\omega}_o$ converges to zero. The uniform continuity of $\boldsymbol{\delta}_o$ implies the convergence of $\boldsymbol{\delta}_o$ to a bounded value, which depends on its initial value.

To analyze the convergence of the payload's center of mass (O) to the target position, we define $\boldsymbol{r}_{i,o}$ as the vector from point O to robot i and $\boldsymbol{\varrho}_o := \sum_{i=1}^{N} \boldsymbol{r}_{i,o}$. We also define $\boldsymbol{e}_o = \boldsymbol{x}_o - \boldsymbol{x}_d$. We can confirm that for a group of robots rigidly attached to a payload,

$$\boldsymbol{r}_c = -\frac{m_r}{m_o}\boldsymbol{\varrho} = -\frac{m_r}{m}\boldsymbol{\varrho}_o. \quad (21)$$

Moreover, since $\boldsymbol{x}_c = \boldsymbol{x}_o - {}^G\boldsymbol{R}_B\boldsymbol{r}_c$, we can write

$$\boldsymbol{e}_c = \boldsymbol{e}_o - {}^G\boldsymbol{R}_B\boldsymbol{r}_c. \quad (22)$$

Substituting Eq. (21) for $\boldsymbol{r}_c$ into Eq. (22) and then incorporating the result into Eq. (13), we obtain

$$\boldsymbol{e}_o^* = -\frac{1}{N}{}^G\boldsymbol{R}_B^*\boldsymbol{\varrho}_o^*, \quad (23)$$

which gives the position error of the payload's center of mass at equilibrium. Like $\boldsymbol{\varrho}$, $\boldsymbol{\varrho}_o$ has a constant magnitude, since the robots are rigidly attached to the payload and O is a fixed point on the payload. Eq. (23) shows that the steady-state distance between the payload's center of mass and the target position depends on the number of robots N and their distribution around the payload. This distance decreases as N is increased, and for payloads with a homogeneous mass density, it decreases as the distribution of robots around the payload's center of mass approaches a uniform distribution. For non-homogeneous payloads, this distance is reduced by allocating the robots in accordance with the payload's mass distribution; e.g., increasing the number of robots around sections of the payload with high mass density. The direction of $\boldsymbol{e}_o^*$ depends on the steady-state value of the payload orientation $\boldsymbol{\delta}_o$ through $\boldsymbol{\varrho}_o^*$; the steady-state orientation depends on the initial value of $\boldsymbol{\delta}_o$, as stated earlier.

4. Simulation Results

In this section, we present MATLAB simulations of our fully decentralized controller for 3D object transport by a team of simulated Astrobee robots in five different scenarios. We assume that the transport task is performed in microgravity,

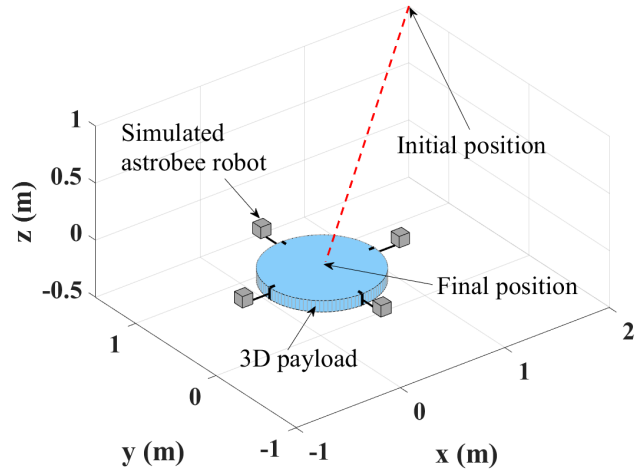

Figure 3: Snapshot of simulation of the first scenario in the steady-state condition. Four Astrobee robots that are symmetrically attached to a cylindrical payload transport it to the origin.

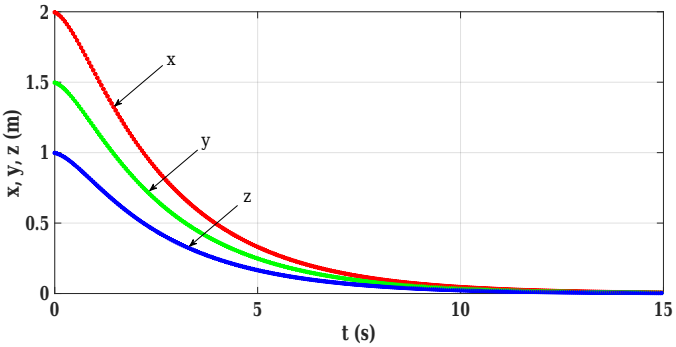

Figure 4: Time evolution of the payload's position in the first scenario.

and that the Astrobees' actuating forces are the only external forces that act on the entire system (the robots and the payload). We also assume that the manipulator of each robot is fixed and that they are rigidly attached to the payload. These assumptions allow us to use the point-mass model described in Section 2 for the dynamics of the Astrobee robots. In all scenarios, the target point is the origin of the orbital coordinate frame. In our figures, we display the simulated Astrobee robots as gray cubes with black manipulators and grippers, the payload as a light blue object, and the trajectory of the payload's center of mass as a red dashed line. Videos of the simulated scenarios are available online in [44].

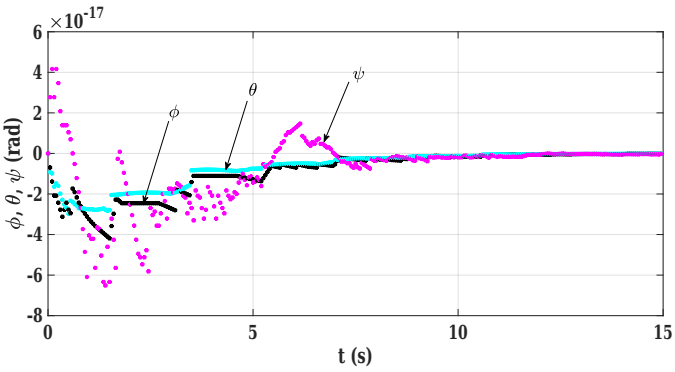

Figure 5: Time evolution of the payload's orientation in the first scenario.

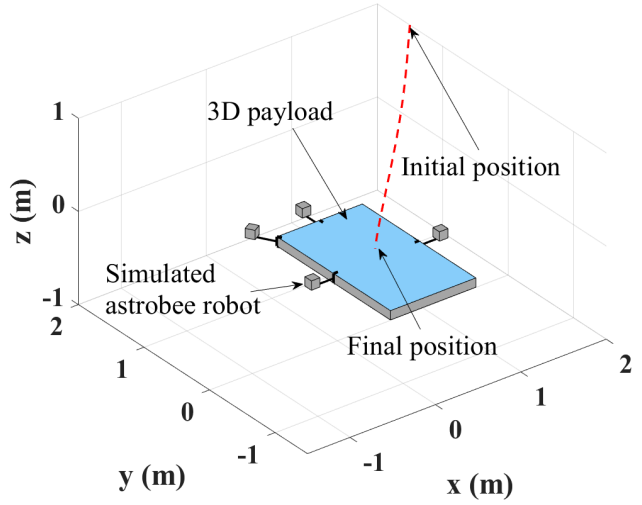

Figure 6: Snapshot of simulation of the second scenario in the steady-state condition. Four Astrobee robots that are asymmetrically attached to a 3D rectangular payload transport it to the origin.

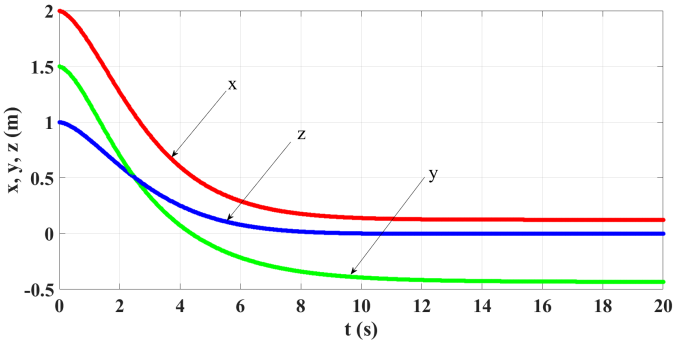

Figure 7: Time evolution of the payload's position in the second scenario.

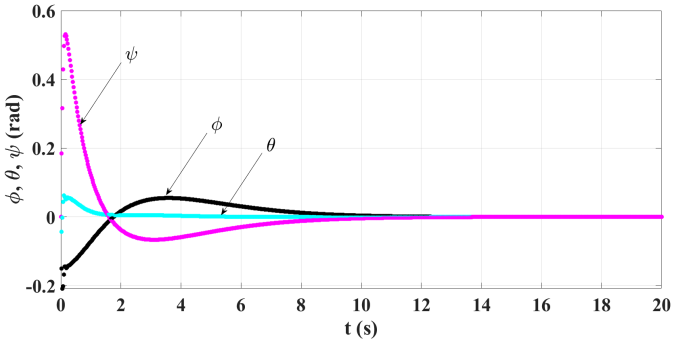

Figure 8: Time evolution of the payload's orientation in the second scenario.

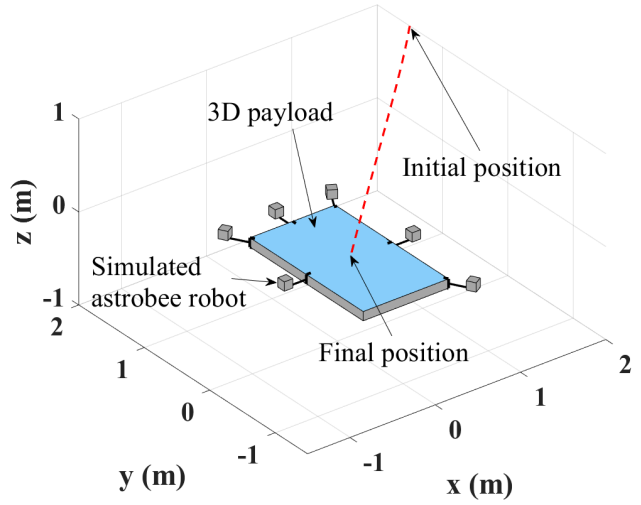

Figure 9: Snapshot of simulation of the third scenario in the steady-state condition. Six Astrobee robots that are asymmetrically attached to a 3D rectangular payload transport it to the origin.

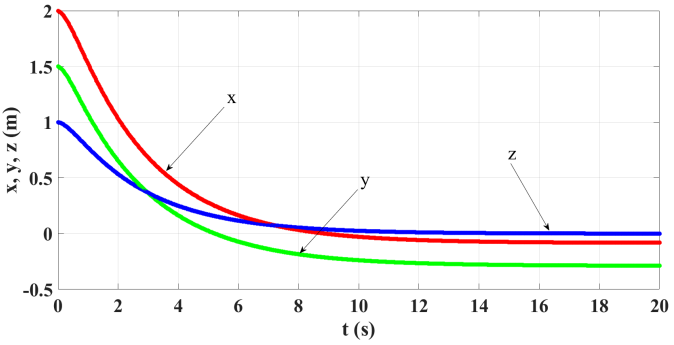

Figure 10: Time evolution of the payload's position in the third scenario.

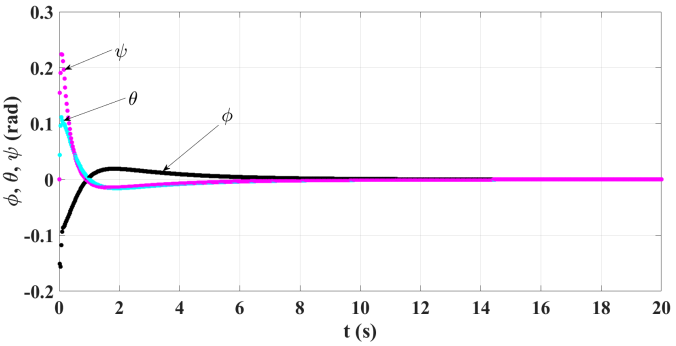

Figure 11: Time evolution of the payload's orientation in the third scenario.

In the first scenario, we simulate a cylindrical payload that is transported by four Astrobee robots. The initial position and orientation of the payload's center of mass are $\boldsymbol{x}_o = [2\ 1.5\ 1]^{\mathrm{T}}$ and $\boldsymbol{\delta}_o = [0\ 0\ 0]^{\mathrm{T}}$. Figure 3 shows a snapshot of the simulation in the steady-state condition. We plot the time evolution of position and orientation of the 3D payload in Figs. 4 and 5. As we discussed in Section 3, the position error of the payload converges to zero since the distribution of the robots around the payload is symmetric.

In the second scenario, we show that if the distribution of robots around the payload is not symmetric, then there is a non-zero steady-state error in the payload's position. Figure 6 shows a snapshot of the simulation where the initial position of the rectangular payload is the same as in the first scenario, while its initial orientation is $\boldsymbol{\delta}_o = [\pi/8\ \ \pi/10\ \ \pi/6]^{\mathrm{T}}$. Although the plots in Fig. 8 show that the payload's orientation converges to zero, its position has a non-zero steady-state error, as shown in Fig. 7, due to the asymmetric distribution of robots around the payload. Recall that this steady-state error can be reduced by increasing the number of robots.

In the third scenario, we increase the number of robots from 4 to 6 and arrange them in an asymmetric distribution around

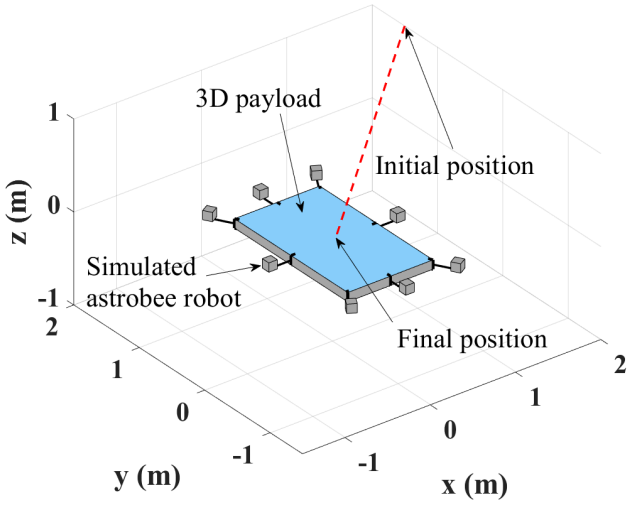

Figure 12: Snapshot of simulation of the fourth scenario in the steady-state condition. Eight Astrobee robots that are symmetrically attached to a 3D rectangular payload transport it to the origin.

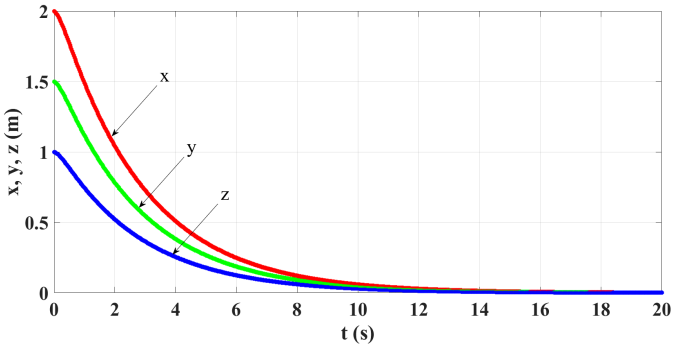

Figure 13: Time evolution of the payload's position in the fourth scenario.

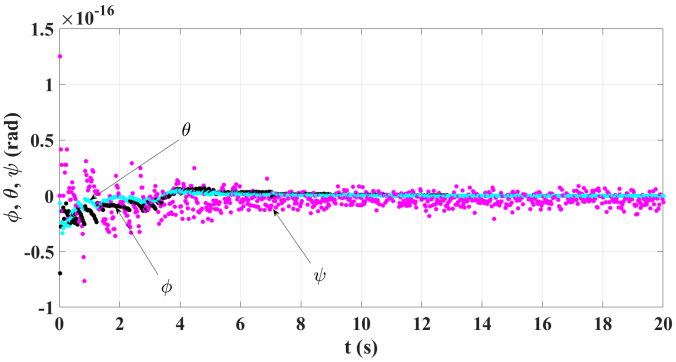

Figure 14: Time evolution of the payload's orientation in the fourth scenario.

the payload. All initial conditions are the same as in the second scenario. Figure 9 shows a snapshot of the simulation in the steady-state condition. As expected, the steady-state error in the payload's position decreases when we add two more robots, as can be seen in Fig. 10. The payload's orientation again converges to zero, as shown in Fig. 11.

In the fourth scenario, we verify that the steady-state error in the payload's position converges to zero if we add two more robots (a total of 8 robots) such that their distribution around the payload becomes symmetric. The initial conditions are

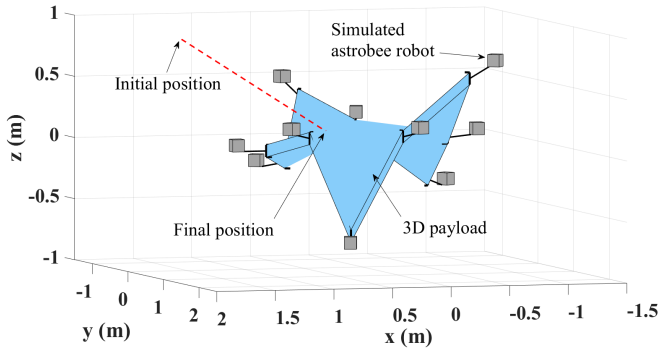

Figure 15: Snapshot of simulation of the fifth scenario in the steady-state condition. Ten Astrobee robots that are asymmetrically attached to a 3D irregular payload transport it to the origin.

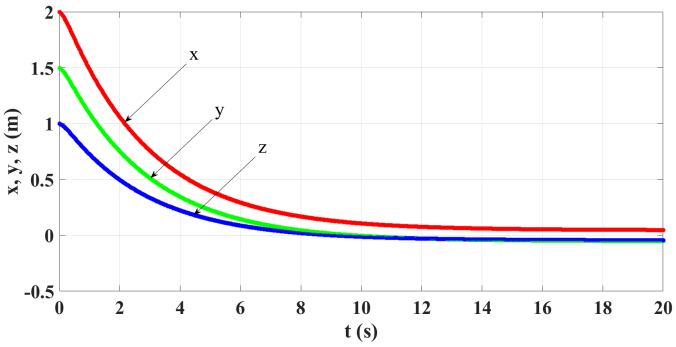

Figure 16: Time evolution of the payload's position in the fifth scenario.

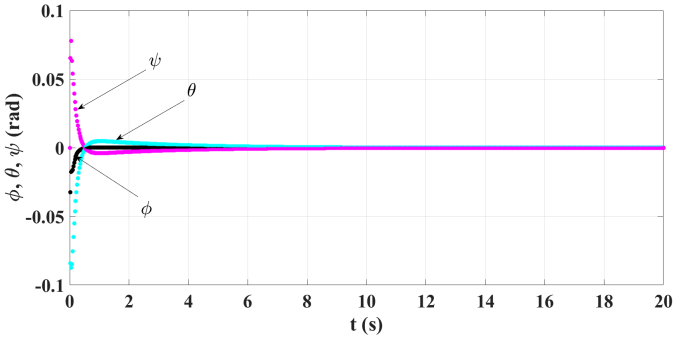

Figure 17: Time evolution of the payload's orientation in the fifth scenario.

the same as in the second and third scenarios. Figure 12 shows a snapshot of the simulation in the steady-state condition. The plots in Figs. 13 and 14 show that the steady-state errors in position and orientation converge to zero.

We also validate our controller for collective transport of an irregular 3D object by a team of 10 Astrobee robots. The initial position and orientation of the payload are the same as in the second, third, and fourth scenarios. Figure 15 shows a snapshot of the simulation, and Figs. 16 and 17 plot the time evolution of the payload's position and orientation. The latter plots show that the position and orientation errors converge to very small values at steady-state. This result indicates that even if the payload has an irregular shape for which there is no symmetric distribution of robots, we can significantly reduce the steady-state error by arranging the robots around the payload boundary in an approximately uniform distribution. We note that the robots' positions over time can be calculated

from the trajectory of the payload, since the robots are rigidly attached to the payload throughout the transport.

5. Conclusion

We have proposed a decentralized PD control strategy for a team of identical point-mass robots to collectively transport a payload in 3D microgravity space to a target position. The controller only requires the robots' local measurements and does not rely on predefined trajectories or explicit communication between the robots. We proved that with the proposed controller, the robots drive the payload to a neighborhood of the destination, where the steady-state distance between the payload's center of mass and the target position is only a function of the number of robots and their distribution around the payload. In future work, we will consider robots with more degrees of freedom in order to use their redundancy to minimize the internal forces that may cause stress in the payload. We will also consider environments with convex obstacles and modify the controller to enable the robots to transport the payload to a destination while avoiding collisions with the obstacles.

References

[1] F. Rossi, S. Bandyopadhyay, M. Wolf, and M. Pavone, "Review of multi-agent algorithms for collective behavior: a structural taxonomy," *IFAC-PapersOnLine*, vol. 51, no. 12, pp. 112–117, 2018.

[2] S. Sabet, M. Poursina, P. E. Nikravesh, P. Reverdy, and A.-A. Agha-Mohammadi, "Dynamic modeling, energy analysis, and path planning of spherical robots on uneven terrains," *IEEE Robotics and Automation Letters*, vol. 5, no. 4, pp. 6049–6056, 2020.

[3] O. Toupet, J. Biesiadecki, A. Rankin, A. Steffy, G. Meirion-Griffith, D. Levine, M. Schadegg, and M. Maimone, "Traction control design and integration onboard the Mars Science Laboratory Curiosity Rover," in *2018 IEEE Aerospace Conference*. IEEE, 2018, pp. 1–20.

[4] W. Xu, B. Liang, D. Gao, and Y. Xu, "A space robotic system used for on-orbit servicing in the geostationary orbit," in *2010 IEEE/RSJ International Conference on Intelligent Robots and Systems*. IEEE, 2010, pp. 4089–4094.

[5] M. G. Bualat, T. Smith, E. E. Smith, T. Fong, and D. Wheeler, "Astrobee: A new tool for ISS operations," in *2018 SpaceOps Conference*, 2018, p. 2517.

[6] M. A. Diftler, J. Mehling, M. E. Abdallah, N. A. Radford, L. B. Bridgwater, A. M. Sanders, R. S. Askew, D. M. Linn, J. D. Yamokoski, F. Permenter *et al.*, "Robonaut 2-the first humanoid robot in space," in *2011 IEEE International Conference on Robotics and Automation*. IEEE, 2011, pp. 2178–2183.

[7] M. G. Richards, "On-orbit serviceability of space system architectures," Ph.D. dissertation, Massachusetts Institute of Technology, 2006.

[8] N. GSFC, "On-orbit satellite servicing study project report," *NASA Project Report NP-2010-08-162-GSFC, Greenbelt, MD*, 2010.

[9] C. Kosmas, "On-orbit-servicing by HERMES on-orbit-servicing system," *KOSMAS GEORING Services, White Paper ver*, vol. 2, 2007.

[10] D. Piskorz and K. L. Jones, "On-orbit assembly of space assets: A path to affordable and adaptable space infrastructure," *The Aerospace Corporation*, 2018.

[11] T. Smith, J. Barlow, M. Bualat, T. Fong, C. Provencher, H. Sanchez, and E. Smith, "Astrobee: A new platform for free-flying robotics on the International Space Station," in *International Symposium on Artificial Intelligence, Robotics, and Automation in Space (i-SAIRAS)*, 2016.

[12] T. J. Czaczkes and F. L. Ratnieks, "Cooperative transport in ants (Hymenoptera: Formicidae) and elsewhere," *Myrmecological News*, vol. 18, pp. 1–11, 2013.

[13] H. F. McCreery and M. Breed, "Cooperative transport in ants: a review of proximate mechanisms," *Insectes Sociaux*, vol. 61, no. 2, pp. 99–110, 2014.

[14] A. Gelblum, I. Pinkoviezky, E. Fonio, N. S. Gov, and O. Feinerman, "Emergent oscillations assist obstacle negotiation during ant cooperative transport," *Proceedings of the National Academy of Sciences*, vol. 113, no. 51, pp. 14 615–14 620, 2016.

[15] O. Medina, S. Hacohen, and N. Shvalb, "Robotic swarm motion planning for load carrying and manipulating," *IEEE Access*, vol. 8, pp. 53 141–53 150, 2020.

[16] J. Leitner, "Multi-robot formations for area coverage in space applications," Ph.D. dissertation, Lulea University of Technology Sweden (LTU), 2009.

[17] M. Goeller, J. Oberlaender, K. Uhl, A. Roennau, and R. Dillmann, "Modular robots for on-orbit satellite servicing," in *2012 IEEE International Conference on Robotics and Biomimetics (ROBIO)*. IEEE, 2012, pp. 2018–2023.

[18] F. W. Heger, L. M. Hiatt, B. Sellner, R. Simmons, and S. Singh, "Results in sliding autonomy for multi-robot spatial assembly," in *International Symposium on Artificial Intelligence, Robotics, and Automation in Space (i-SAIRAS)*, 2005.

[19] G. Rekleitis and E. Papadopoulos, "On-orbit cooperating space robotic servicers handling a passive object," *IEEE Transactions on Aerospace and Electronic Systems*, vol. 51, no. 2, pp. 802–814, 2015.

[20] J. Chen, M. Gauci, W. Li, A. Kolling, and R. Groß, "Occlusion-based cooperative transport with a swarm of miniature mobile robots," *IEEE Transactions on Robotics*, vol. 31, no. 2, pp. 307–321, 2015.

[21] A. Franchi, A. Petitti, and A. Rizzo, "Distributed estimation of the inertial parameters of an unknown load via multi-robot manipulation," in *Proc. IEEE International Conference on Decision and Control*, Dec 2014, pp. 6111–6116.

[22] A. Marino, G. Muscio, and F. Pierri, "Distributed cooperative object parameter estimation and manipulation without explicit communication," in *Proc. IEEE International Conference on Robotics and Automation (ICRA)*, May 2017, pp. 2110–2116.

[23] P. B. G. Dohmann and S. Hirche, "Distributed control for cooperative manipulation with event-triggered communication," *IEEE Transactions on Robotics*, vol. 36, no. 4, 2020.

[24] H. Lee, H. Kim, and H. J. Kim, "Planning and control for collision-free cooperative aerial transportation," *IEEE Transactions on Automation Science and Engineering*, vol. 15, no. 1, pp. 189–201, 2016.

[25] A. Marino, "Distributed adaptive control of networked cooperative mobile manipulators," *IEEE Transactions on Control Systems Technology*, vol. 26, no. 5, pp. 1646–1660, 2017.

[26] J. Pliego-Jimenez and M. Arteaga-Perez, "On the adaptive control of cooperative robots with time-variant holonomic constraints," *International Journal of Adaptive Control and Signal Processing*, vol. 31, no. 8, pp. 1217–1231, 2017.

[27] S. Kim, H. Seo, J. Shin, and H. J. Kim, "Cooperative aerial manipulation using multirotors with multi-dof robotic arms," *IEEE/ASME Transactions on Mechatronics*, vol. 23, no. 2, pp. 702–713, 2018.

[28] H. Lee, H. Kim, W. Kim, and H. J. Kim, "An integrated framework for cooperative aerial manipulators in unknown environments," *IEEE Robotics and Automation Letters*, vol. 3, no. 3, pp. 2307–2314, 2018.

[29] G. B. Dai and Y. C. Liu, "Distributed coordination and cooperation control for networked mobile manipulators," *IEEE Transactions on Industrial Electronics*, vol. 64, no. 6, pp. 5065–5074, June 2017.

[30] P. Culbertson, J.-J. E. Slotine, and M. Schwager, "Decentralized adaptive control for collaborative manipulation of rigid bodies," *arXiv preprint arXiv:2005.03153*, 2020.

[31] P. Culbertson and M. Schwager, "Decentralized adaptive control for collaborative manipulation," in *Proc. IEEE International Conference on Robotics and Automation (ICRA)*, May 2018, pp. 278–285.

[32] Z. Li, C. Yang, C. Y. Su, S. Deng, F. Sun, and W. Zhang, "Decentralized fuzzy control of multiple cooperating robotic manipulators with impedance interaction," *IEEE Transactions on Fuzzy Systems*, vol. 23, no. 4, pp. 1044–1056, Aug 2015.

[33] A. Marino and F. Pierri, "A two stage approach for distributed cooperative manipulation of an unknown object without explicit communication and unknown number of robots," *Robotics and Autonomous Systems*, vol. 103, pp. 122 – 133, 2018.

[34] H. Bai and J. T. Wen, "Cooperative load transport: A formation-control perspective," *IEEE Transactions on Robotics*, vol. 26, no. 4, pp. 742–750, Aug 2010.

[35] F. Pierri, M. Nigro, G. Muscio, and F. Caccavale, "Cooperative manipulation of an unknown object via omnidirectional unmanned aerial vehicles," *Journal of Intelligent & Robotic Systems*, vol. 100, no. 3, pp. 1635–1649, 2020.

[36] L. Jin, S. Li, X. Luo, Y. Li, and B. Qin, "Neural dynamics for cooperative control of redundant robot manipulators," *IEEE Transactions on Industrial Informatics*, vol. 14, no. 9, pp. 3812–3821, 2018.

[37] X. Li, Z. Xu, S. Li, H. Wu, and X. Zhou, "Cooperative kinematic control for multiple redundant manipulators under partially known information using recurrent neural network," *IEEE Access*, vol. 8, pp. 40 029–40 038, 2020.

[38] G. Ding, J. J. Koh, K. Merckaert, B. Vanderborght, M. M. Nicotra, C. Heckman, A. Roncone, and L. Chen, "Distributed reinforcement learning for cooperative multi-robot object manipulation," in *Proc. of the 19th International Conference on Autonomous Agents and MultiAgent Systems (AAMAS)*, 2020, p. 1831–1833.

[39] H. Farivarnejad and S. Berman, "Stability and convergence analysis of a decentralized proportional-integral control strategy for collective transport," in *Proc. American Control Conference (ACC)*, June 2018, pp. 2794–2801.

[40] ——, "Decentralized PD control for multi-robot collective transport to a target location using minimal information," in *Unmanned Systems Technology XXII*, vol. 11425. International Society for Optics and Photonics, 2020, p. 1142506.

[41] H. Farivarnejad, S. Wilson, and S. Berman, "Decentralized sliding mode control for autonomous collective transport by multi-robot systems," in *Proc. IEEE International Conference on Decision and Control (CDC)*, Dec 2016, pp. 1826–1833.

[42] R. M. Murray, S. S. Sastry, and L. Zexiang, *A Mathematical Introduction to Robotic Manipulation*, 1st ed. Boca Raton, FL, USA: CRC Press, Inc., 1994.

[43] H. K. Khalil, *Nonlinear Systems*. Upper Saddle River, N.J.: Prentice Hall, 1996.

[44] Autonomous Collective Systems Laboratory YouTube channel, "Fully decentralized controller for multi-robot collective transport in space applications," https://www.youtube.com/watch?v=dArcY3dVdZQ, 2020.